Compressive Sensing based Single-Pixel Hyperspectral Camera

Liang Shi
Stanford University
liangs@stanford.edu

Shihkar Shrestha
Stanford University
shikhars@stanford.edu

Abstract

In this report, we propose a novel compressive hyperspectral(HS) imaging approach which extends the single-pixel camera structure to be applicable for acquiring hyperspectral data. We build a hardware prototupe using modified DLP based spatial light modulator, OceanOptics USB4000-VIS-NIR spectrometer and Lumencor fiber coupled light engine. We also design an ADMM based reconstruction algorithm and show successful recovery of HS images on both synthetic and real-captured data. In addition, we simulate the HS image reconstruction using spectrometer measurements plus RGB image which gives a more accurate and edge-preserved result under same measurement rate.

1. Introduction

Hyperspectral(HS) image is 3D datacube storing the intensity of light as a function of wavelength λ at each spatial location (x, y). The spectrum distribution revealled by the hyperspectral image is useful in identifying the composition and structure of objects and the environment lightings. Many real applications have been widely used in agriculture, mineralogy, surveillance and so on.

In order to capture 3D HS image, conventional approaches always require some form of temporal scanning in either spatial domain or spectral domain. A dispersive pushbroom slit spectromter simultaneously acquires a slit of spatial information, as well as spectral information corresponding to each spatial point in the slit for one scan. Capturing the entire datacube relies on spatial motion of either the spectrometer or the object. A tunable spectral filter imager takes multiple images of the same scene sequentially in different bandpass settings. As a result, all these methods require a relatively long acquisition time and huge amount of space for data storage due to the full measurement.

Recently, a new theory known as compressive sensing(CS) has emerged. The basic idea of this theory is when the signal of interest is very sparese(i.e. zero-valued at most locations) or highly compressible in some basis, relatively few incoherent observations will be enough to reconstruct a close estimation of the signal. The CS theory provides a sensing framework for sampling sparse or compressible signals in a more efficient way that is usually done with Shannon Nyquist sampling scheme. One natural implementation arena of CS theory is the field of imaging.

Borrowing idea from this theory, we propose a HS imager that records the light signal with a single detection element, however, without acquiring spectrum of each pixel squentially. Instead of scanning, a digital micromirror device(DMD) randomly but controllably modulates the light from the scenes which is then summed before reaching the detector. Since it optically realizes the random measurements described in CS theory, we can use far fewer observations than the total number of pixels to recover the entire datacube. As a result, it dramatically decreases the data acquisition time and space for data storage. In addition, the intensity of the compressed signal at the detector is much greater with respect to raster scan and therefore results in greater signal sensitivity.

In particular, we make the following technical contributions:

- We proposed an extended single-pixel camera structure for capturing HS image using modified DLP projecter, USB4000-VIS-NIR portable spectrometer, and Lumencor fiber coupled light engine.
- We introduce an ADMM based reconstruction algorithm for solving the sparse-constrained optimization problem. We give simulation result on 5 different measurement matrices with 5 different priors.
- Though theoretically simulated by previous papers, we are by far the first group build up the hardware prototype and successfully reconstruct the HS image from real-captured data.
- We simulate the HS image reconstruction using spectrometer measurements plus RGB image, and show it gives a more accurate and edge-preserved result under same measurement rate.

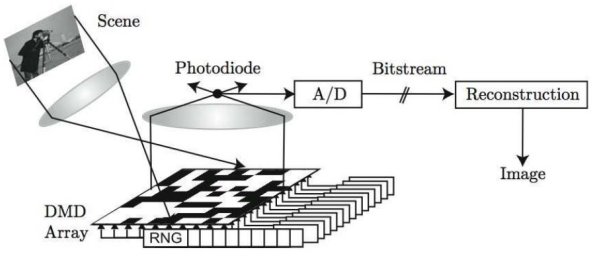

Figure 1. Single-pixel camera

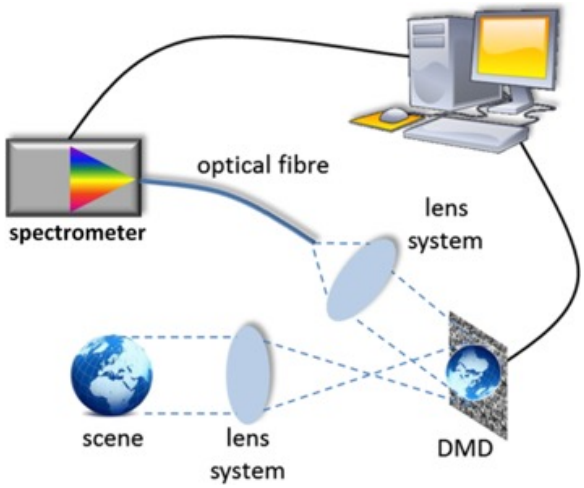

Figure 2. Single-pixel hyperspectral camera

2. Related Work

In 2006, Rice University brought up the first implementation of CS for imaging — the single-pixel camera[1]. It's hardware setup is showed in Fig. 1. With the help of biconvex lens, the desired image is first projected to on the DMD plane. At the same time, a random pattern is generated on the DMD by controlling the state(+12 degrees or -12 degrees) of electrostatically actuated micromirrors. All the "on" micromirrors redirect the lights through the second biconvex lens which focuses the coded image onto the photodiode. For each random pattern, the photodiode will yield an absolute voltage measurement as the summed intensity of all the pixels in coded image. If the desired image has size $N = w \times h$, by taking M measurements that $M \ll N$, we can still reconstruct the gray image with the sparse priors.

Recently, a series of CS based snapshot HS imaging systems have been proposed[2,3,4,5,6]. In 2007, a method called dual-disperser coded aperture snapshot spectral imager(DD-CASSI)[2] first introduced the CS into HS imaging. In the DD-CASSI architecture, the light is spectrally sheared by the first prism, then coded by the mask on aperture, finally unsheared by the second prism. The measurements is captured by a 2D CCD array which records

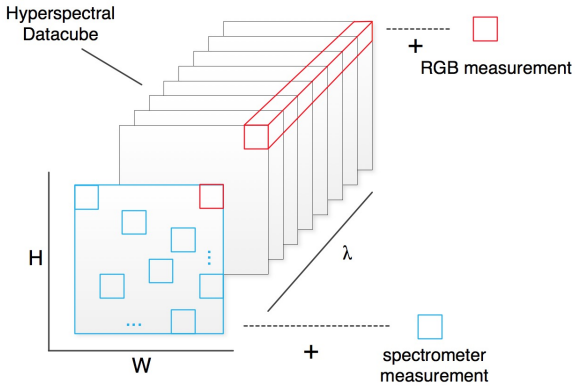

Figure 3. Demonstration of two different measurements

the weighted sum of all the coded slices along λ-axis. Later, the SD-CASSI[3] architecture is developed by removing the first dispersive arm in DD-CASSI. It sacrifices the spectral multiplexing in DD-CASSI in exchange for the spatial multiplexing. Meanwhile, it reduces the optical elements in the entire system. In 2011, a DMD-SSI[4] system came up by replacing the coded aperture with the DMD. When reconstructing with multiple shots, DMD-SSI can introduce more randomness, whereas previous approaches only provide a shifted patterns. In 2014, Xing Lin proposed a spatial-spectral encoded snapshot spectral imager[5] which achieves spatial-spectral modulation by simpliy putting a coded mask between the spectral plane and CCD sensor in his architecture.

Another concept of CS based HS imaging system, which is also the one implemented in our report, is proposed in [6] at 2009. Fig. 2 shows the difference between this method with single-pixel camera. Basically, it extends the single-pixel camera structure by replacing the photodiode with a spectrometer probe. In this architecture, the spatial information is encoded and parallelly measured as the spectral curve. However, this two and a half pages COSI paper does not give any illustration for the hardware setup and reconstruction algorithm. Thus, in our project, all the hardware prototype and reconstruction algorithms are designed from scratch.

3. Model

In this section, we will mathematically formulate our data capturing process. In addition, we provide a detailed illustration of how CS playing its role in this task by generalizing all the measurements into a sparse-contrained optimization problem.

3.1. Spectrometer Measurement

Fig. 3 gives an intuitive demonstration of how the data is captured along two different dimensions. First, let's focus on the spectrometer measurements. Assume the grouth-

truth data G has size $\mathbb{R}^{W\times H\times S}$, where $W \times H$ is the image size and S is the total number of slices along λ. Let $\{g_1, g_2, \ldots, g_S\}$ be the images at each slice and m be the total number of measurements. We can mathematically represent the acquisition of spectrometer measurements in the following steps:

- initialize $i = 1$
- generate an $\mathbb{R}^{W\times H}$ mask M_i using certain rules(i.e. random binominal)
- Multiply M_i element-wisely with $\{g_1, g_2, \ldots, g_S\}$ to obtain the coded images $\{c_{i1}, c_{i2}, \ldots, c_{iS}\}$
- For each of $\{c_{i1}, c_{i2}, \ldots, c_{iS}\}$, sum the all the elements inside to obtain the single pixel observation $\{o_{i1}, o_{i2}, \ldots, o_{iS}\}$
- $i = i + 1$, repeat until $i = m$

Notice, measurements from spectrometer are the summation of pixel values in spatial domain not in spectral domain.

3.2. RGB measurement

To impose constraint on spectral dimension, we can capture an RGB image for the target scene. It can be simulated by applying CIE function to the hyperspectral datacube. For the time limitation, we simulate a more simplified version which takes the weighted sum of all the slices to generate a gray image. However, the basic idea is similar and it exerts the same effect as the RGB image. Here, we denote $\{w_1, w_2, ..., w_S\}$ as the weights for each slice and Q as an $\mathbb{R}^{WH\times 1}$ column vector reshaped by the gray image we capture.

3.3. CS Formulation

Now, we have both spectrometer measurements and gray image. If we only use the measurements from spectrometer, there are two ways to put all the data into a compressive sensing feasible form. Since the parameters in the first expression will be the building blocks in the second, we introduce that first,

$$\min_{x_j} ||Hx_j||_1, \quad s.t.\ Ax_j - b_j = 0,\ j \in \{1, 2, \ldots, S\} \quad (1)$$

Here, A is the an $\mathbb{R}^{m\times n}$ matrix with $n = W \times H$. It is formed by stretching each M_i into a row vector and stacking all of them vertically. b_j is an $\mathbb{R}^{m\times 1}$ column vector formed by stacking all o_{ij} vertically. x_j is an $\mathbb{R}^{n\times 1}$ column vector reshaped by g_j.

In this expression, the datacube reconstruction is partitioned into several individual problems as reconstructing each slice by slice. One advantage of solving in this form is we can initialize the guessing of next slice with previous reconstructed one which is reasonable for the spectral smoothness. As neighbour slices will be similar to each other, the iterations to convergence will dramatically decrease(almost 50 %). However, since the entire datacube is decomposed into slices, sparse priors like 3DTV become impossible to fit in this form. In addition, the gray(or RGB) image measurement is also unable to add in the form since it has to be expressed as the weighted sum of all the slices. Thus, we give the second and more concept-coherent formulation which reconstructs the datacube at once,

$$\min_X ||HX||_1, \quad s.t.\ A^*X - B = 0 \quad (2)$$

$$X = \begin{bmatrix} x_1 \\ x_2 \\ \vdots \\ x_S \end{bmatrix}, \quad B = \begin{bmatrix} b_1 \\ b_2 \\ \vdots \\ b_S \\ Q \end{bmatrix} \quad (3)$$

$$A^* = \begin{bmatrix} A & & & \\ & A & & \\ & & \ddots & \\ & & & A \\ W_1 & W_2 & \cdots & W_S \end{bmatrix} \quad (4)$$

$$W_i = \begin{bmatrix} w_i & & & \\ & w_i & & \\ & & \ddots & \\ & & & w_i \end{bmatrix} \quad (5)$$

Here, W_i is an $\mathbb{R}^{n\times n}$ matrix with all diagonal elements equal to w_i. This formulation incorporates the gray image measurement and we can remove that by deleting the W row in A^* and Q in B. In both formulations, the underdetermined equations can be solved by finding the sparsest solution in certain sparese domain and it is also known as the sparse priors.

In our simulation, we implement five different measurement matrices with 5 different sparse priors,

Sensing Matrix

1. random binomial
2. random Guassian
3. permutated DCT
4. permutated DFT
5. permutated discrete Walsh-Hadamard transform

Sparse Priors

a. isotropic 2D TV(total variation)

b. anisotropic 2D TV

c. DCT

d. wavelet(haar)

e. 3D TV

4. ADMM based Reconstruction

In our project, we use the alternating direction method of multipliers(ADMM) to solve the sparse-constrained optimization problem. Since equation (1) and (2) try to optimize the same kind of problem with only difference in the matrices size, we rewrite the problem with different annotations to eliminate the ambiguity of using either of them.

$$\min_u \sum_i ||D_i u||, \quad s.t.\ Au = b \tag{6}$$

Here, the term we try to minimize is defined as a summation of u's norm in several sparse basis, it is considered for the sparse priors like anisotropic TV which consists of first derivative along both X-axis and Y-axis (and λ-axis in 3DTV). Now, we consider the equivalent variant of (3),

$$\min_{w_i,u} \sum_i ||w_i||, \quad s.t.\ Au = b \text{ and } D_i u = w_i \text{ for all } i \tag{7}$$

its corresponding augmented Lagrangian function is,

$$\min_{w_i,u} \mathcal{L}_A(w_i, u) = \sum_i (||w_i|| - \nu_i^T (D_i u - w_i) + \frac{\beta_i}{2}||D_i u - w_i||_2^2) + \frac{\mu}{2}||Au - b||_2^2 \tag{8}$$

The ADMM solves this problem by sequentially updating each parameter while fixing the others. In our problem, each iteration consists of 3 steps as updating w_i, u, ν respectively.

Assume u_k, $w_{i,k}$ and $\nu_{i,k}$ are the approximate minimizers of (5) at the kth iteration. We first update $w_{i,k+1}$ by

$$\min_{w_i} \mathcal{L}_A(w_i, u_k) = \sum_i (||w_i|| - \nu_{i,k}^T (D_i u_k - w_i) + \frac{\beta_i}{2}||D_i u_k - w_i||_2^2) + \frac{\mu}{2}||Au_k - b||_2^2 \tag{9}$$

which is equivalent to

$$\min_{w_i} \sum_i (||w_i|| - \nu_{i,k}^T (D_i u_k - w_i) + \frac{\beta_i}{2}||D_i u_k - w_i||_2^2) \tag{10}$$

Except from isotropic TV, all the other sparese priors try to minimize the $L1$ norm of w_i. Notice, the update is separable with respect to each w_i, so the minimizer of

$$\min_{w_i} ||w_i||_1 - \nu_{i,k}^T (D_i u_k - w_i) + \frac{\beta_i}{2}||D_i u_k - w_i||_2^2 \tag{11}$$

is given by 1D shrinkage-like formula,

$$w_{i,k+1} = \max\{|D_i u_k - \frac{\nu_{i,k}}{\beta_i}| - \frac{1}{\beta_i}, 0\} sgn(D_i u_k - \frac{\nu_{i,k}}{\beta_i}) \tag{12}$$

In isotropic TV, we actually minimize the $L2$ norm of w_i, the minimizer of

$$\min_{w_i} ||w_i||_2 - \nu_{i,k}^T (D_i u_k - w_i) + \frac{\beta_i}{2}||D_i u_k - w_i||_2^2 \tag{13}$$

is given by 2D shrinkage-like formula,

$$w_{i,k+1} = \max\{|D_i u_k - \frac{\nu_{i,k}}{\beta_i}| - \frac{1}{\beta_i}, 0\} \frac{D_i u_k - \nu_{i,k}/\beta_i}{||D_i u_k - \nu_{i,k}/\beta_i||} \tag{14}$$

Next, we use $w_{i,k+1}$ to update u_{k+1} as

$$\min_u \mathcal{L}_A(w_{i,k+1}, u) = \sum_i (||w_{i,k+1}|| - \nu_{i,k}^T (D_i u - w_{i,k+1}) + \frac{\beta_i}{2}||D_i u - w_{i,k+1}||_2^2) + \frac{\mu}{2}||Au - b||_2^2 \tag{15}$$

which is equivalent to

$$\min_u \sum_i (-\nu_{i,k}^T (D_i u - w_{i,k+1}) + \frac{\beta_i}{2}||D_i u - w_{i,k+1}||_2^2) + \frac{\mu}{2}||Au - b||_2^2 \tag{16}$$

Notice, it's a quadratic function and its gradient is

$$d_k(u) = \sum_i (\beta_i D_i^T (-D_i u - w_{i,k+1}) - D_i^T \nu_{i,k}) + \mu A^T (Au - b) \tag{17}$$

By setting the gradient to zero, we can obtain the exact minimizer,

$$u_{k+1}^* = \left(\sum_i \beta_i D_i^T D_i + \mu A^T A \right)^+ \left(\sum_i (D_i^T \nu_{i,k} + \beta_i D_i^T w_{i,k+1}) + \mu A^T b \right) \tag{18}$$

where the $^+$ denotes the pseudoinverse of matrix. In practice, it is computationally intractable to compute the inverse

or pseudoinverse even for the image with a comparatively small size(i.e. 128×128). Instead, we adopt one-step gradient descent to get an approximate minimizer

$$u_{k+1} = u_k - \alpha_k d_k \tag{19}$$

where α_k can be determined by Barzilai and Borwein method[7], which suggests

$$\alpha_k = \frac{(u_k - u_{k-1})^T (u_k - u_{k-1})}{(u_k - u_{k-1})^T (d_k - d_{k-1})} \tag{20}$$

Experiments show one-step gradient descent has good astringency and can dramatically speed up the calculation. Since pixel value in an image should be greater than zero, we perform non-negative projection for all the elements in u after every update,

$$u_{k+1} = max(u_{k+1}, 0) \tag{21}$$

Finally, we update the multipliers which is trivial comparing with previous steps

$$\nu_{i,k+1} = \nu_{i,k} - \beta_i (D_i u_{k+1} - w_{i,k+1}) \tag{22}$$

We keep updating until the relative change $\frac{||u_{k+1} - u_k||}{||u_k||}$ is sufficiently small. The final u will be our best estimation for the sparse-contrained optimization problem.

5. Simulation Result

In this section, we exhaustively evaluate the reconstruction result using simulated data and try to gain some on insight how to choose the parameters to achieve best reconstruction result.

Experiment 1

In the first experiment, we test all the possible combination of measurement matrices and sparsity priors. The setting of experiment is

- Use "Balloon" set from Columbia Multispectral Image Database
- Only reconstruct a single slice(thus no 3DTV prior)
- no image downsampling
- measurement rate: 30%, 10%, 3%
- no additive noise
- no test on random Guassian matrix; 20 activated positions for each row of random binomial matrix

Notice, we do not test on random Guassian matrix at the original scale since multiplication with it takes $O(N^2)$ which is intractable when $N = 512^2$. The random binomial matrix is feasible at that scale because we only need to turn on few pixels(i.e. 20) for each mask to get a good result. All the combinations are expressed using symbols assigned in section 3.3.(i.e. (1,a) = (random binomial, isotropic 2D TV))

Combo	30% measurement		
	Rel_Err(%)	PSNR(db)	CPU time(s)
(1,a)	1.15	51.25	18.33
(1,b)	1.33	49.22	17.89
(1,c)	4.52	38.87	33.65
(1,d)	3.18	42.88	27.31
(3,a)	4.15	40.35	6.20
(3,b)	4.17	40.31	6.02
(3,c)	11.24	31.56	52.48
(3,d)	11.02	31.81	65.8
(4,a)	3.23	42.53	5.84
(4,b)	3.23	42.53	5.41
(4,c)	7.42	35.32	89.60
(4,d)	7.73	35.06	78.63
(5,a)	4.14	40.36	4.10
(5,b)	4.15	40.35	3.89
(5,c)	10.93	31.92	33.23
(5,d)	10.68	32.12	52.37
Combo	10% measurement		
	Rel_Err(%)	PSNR(db)	CPU time(s)
(1,a)	2.54	44.62	15.48
(5,a)	7.01	35.87	9.08
Combo	3% measurement		
	Rel_Err(%)	PSNR(db)	CPU time(s)
(1,a)	6.12	36.91	20.12
(5,a)	11.25	31.87	16.65

As shown in table, the isotropic 2D TV consistently yields the lowest reconstruction error. At the scale of 512×512, random binomial measurement matrix with isotropic TV gives the highest PSNR. However, random Guassian matrix has been proved with best RIP properties and we test it at the scale of 128×128 which does give slightly higher accuracy. However, the random binomial matrix is the only one that otpically feasible.

Experiment 2

In this experiment, we focus on reconstructing the entire datacube. As mentioned, in the first formulation, we can accelerate the reconstruction by initializing the guessing of current slice with previously reconstructed one. Now, we show the comparison between this strategy with random guessing initialization on reconstructing $512 \times 512 \times 31$ datacube. In addition, we also test the reconstruction using the second formulation. For all the strategies, we run experiments on the "Beads" data with 10% measurement.

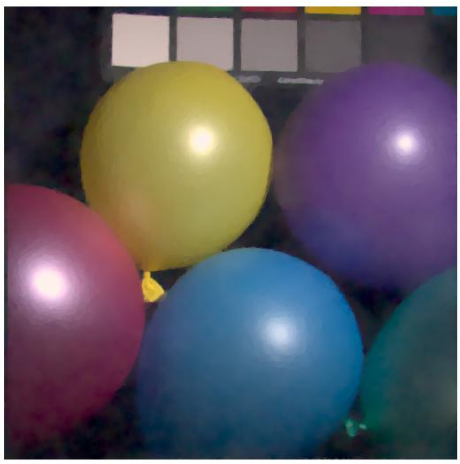

Figure 4. Result of (1,a) with 3% measurement

Figure 5. Result of (1,a) with 10% measurement

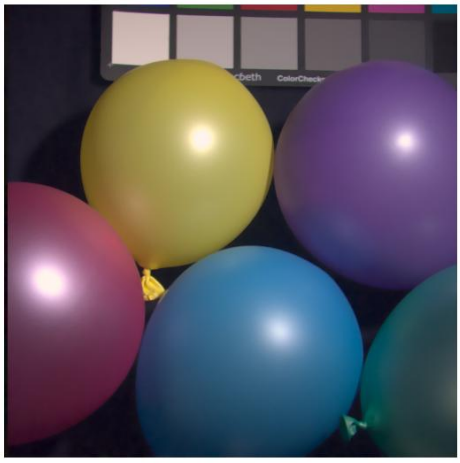

Figure 6. Result of (1,a) with 30% measurement

Figure 7. Result of 2D TV with 10% measurement+gray image

Figure 8. Result of 3D TV with 10% measurement+gray image

For the first formulation, we test two different initializtions with combo (1,a). For the second, we test (1,a) and (1,e) with both random initializtion(cannot pre-initialize). We run experiments for 5 times, and the results shown below are the averaged performance. For fair comparison, we do not count the time for generating the measurement matrix.

strategy	Rel_Err(%)	CPU time(s)
(1,a) & guessing	33.37	402.4
(1,a) & pre-init	33.32	168.6
(1,a) & formulation 2	14.14	250.24
(1,e) & formulation 2	18.52	255.68

As shown, using pre-initializtion dramatically decreases the calculation time and produces similar result. On the other hand, with the additional contraint imposed by gray image, the reconstruction results produced by formulation 2

Figure 9. Result of 2D TV with 10% measurement

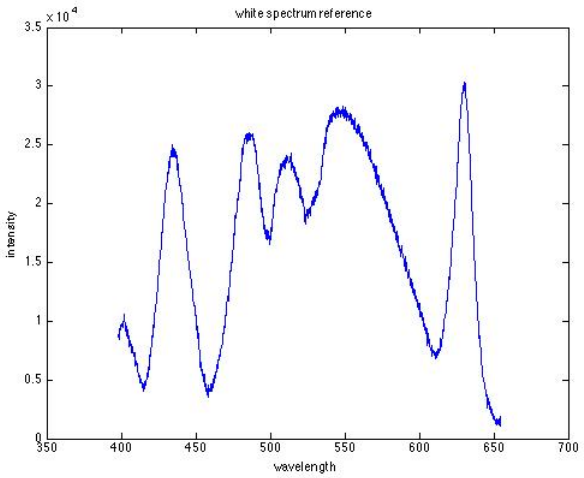

Figure 11. White light spectrum reference

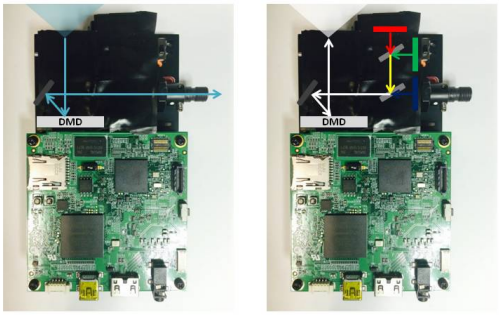

Figure 10. Left: modified; Right: original

get a hugh improve which is equivalent to the one obtained by 30% measurement and only spectrometer measurement. Notice, the performance of 3DTV is worse than 2DTV, it may caused by the excessive smoothing effect imposed along the λ-axis. We can mitigate this effect by tuning the weight for this sparse component.

6. Prototype

6.1. Hardware Setup

To verify our model, we build up the hardware setup for capturing real data. There are three core components in our setup: spatial light modulator(SLM), spectrometer and light source. The basic idea is to light up the scene, use SLM to turn on specfic pixels in the sence and redirect them to the spectrometer, which will measure the spectrum distribution.

As shown in the Fig. 10, we modify the TI LightCrafter 4500 to be our SLM since it consists of a DMD and control electronics in an integrated development platform. It is originally designed for light projection and consists of a light engine that integrates RGB LEDs and projection optics. To convert it into a light collector, we remove the LEDs and also the dichroic mirrors to prevent clipping of the spectrum. In addition, we installed a collimating lens (74-series) made by Ocean Optics with a 10mm focal length to direct as much light as possible into the fiber (400um core diameter), which couples the light into the spectrometer.

Ocean Optics USB4000 UV-VIS spectrometer is used in the setup for its portability and compatibility with MATLAB. The spectrometer supports the spectrum from 200-850 nm, however, the coating on DMD limits the system to operate in visible range(400-650 nm).

To capture hyperspectral data, we also need a powerful light source that emits light in the entire spectral range of interest. The Lumencor fiber coupled light engine is used for this setup and configured to approximate a broad band white light source. The settings for different LEDs are shown below:

- Violet - 100
- Blue - 100
- Cyan - 53
- Teal - 100
- Green - 21
- Red - 22

Fig. 11 shows the white light spectrum captured by the spectrometer in above settings with 20% on-pixels on the DMD.

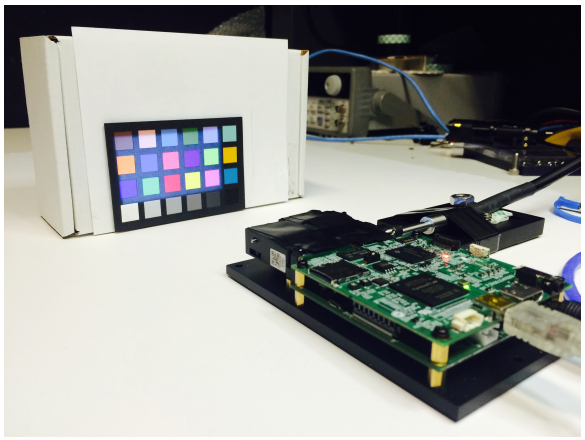

Figure 12. Setup in view calibration mode

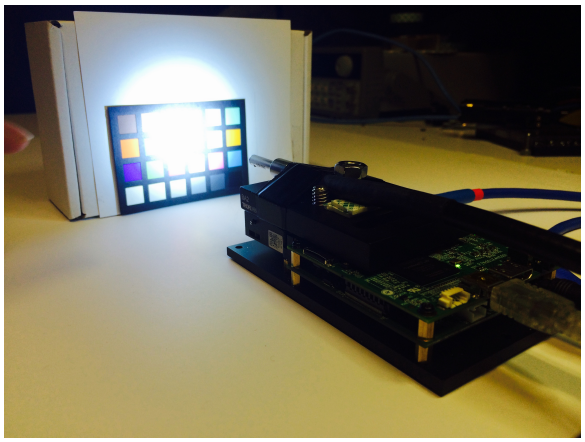

Figure 13. Setup in data acquisition mode

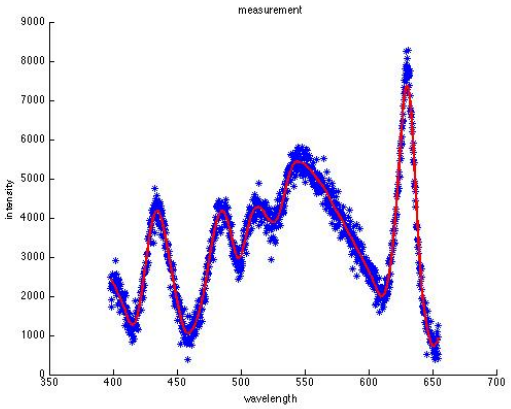

Figure 14. Spectrometer measurement & fitted curve

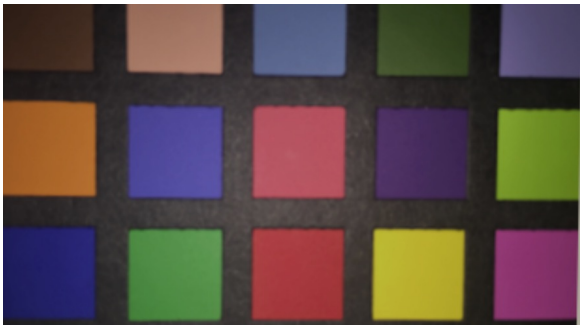

Figure 15. Target scene

6.2. Data Capture

Before capturing the data, we first need to calibrate the scene to determine the field of view. Fig. 12 shows the setup in view calibration mode. It is done by coupling the light into DMD and adjusting the scene to be fully illuminated by the light projected from the LightCrafter. Meanwhile, we upload some random coded masks to examine if the DMD works normally.

Once we determine the field of view, the light source can be used to illuminate the scene and the fiber optic connector for the spectrometer is connected to the lens for data acquisition. Fig. 13 shows the setup in data acquisition mode. In practice, we turn off the room illumination to provent background noise. During the measurement, we generate random patterns in MATLAB and switch the DMD based on the intergration time of spectrometer.

In our experiment, we use 600×600 sub-region on the DMD. Every 20×20 pixels are combined to be a superpixel, which leads to a 30×30 image. This operation allows more lights to come in the spectrometer, thus decreases the integration time for each measurement. The low resolution image also requires less measurements under same measurement rate. Here, the integration time we use for each measurement is 150ms. The measurement rate is 50%.

6.3. Data preprocessing

Each measurement from the spectrometer is stored as two 3648×1 vectors with one representing the wavelength, the other representing the intensity. As shown in the Fig. 14, the captured raw data is very noisy, thus we have to fit a curve for those points. Here, we use *smooth* function in MATLAB with smoothing factor equals to 0.1. The fitted curve is also shown in Fig. 14. After that, we take 26 samples from 400-650 nm with every 10 nm. By dividing them with the white reference intensity respectively, we obtain the pre-processed measurement for the reconstruction algorithm.

7. Result from Real-data

We choose 2D TV as the sparse prior for reconstructing the real-data. The target scene and reconstruction result are shown in Fig. 15 and Fig. 16 respectively. As shown, all the colors on the checkerboard are correctly reconstructed. Though the image resolution is low, we can clearly identify the boundaries between each blocks. Fig. 17 shows the

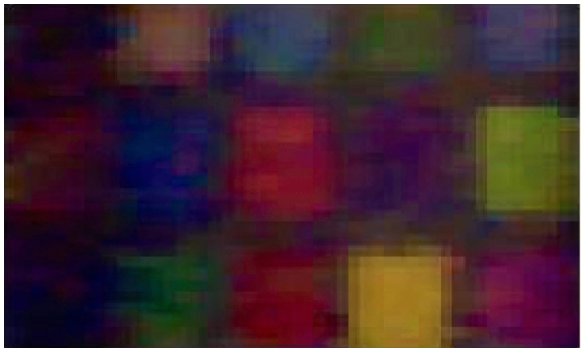

Figure 16. Reconstruction result

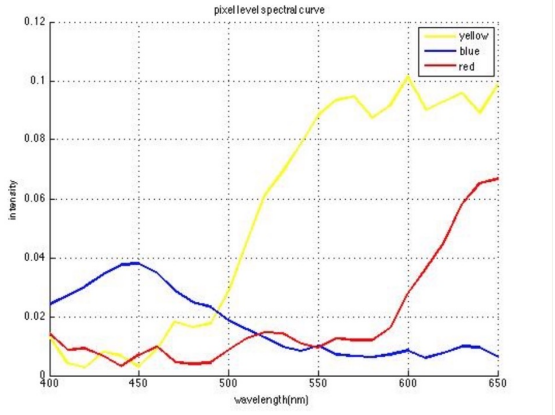

Figure 17. Spectrum curve

spectral curve recovered for the yellow, red and blue blocks. All the peaks show up at the correct wavelength. Since we do not have the low-resolution ground-truth, we did not calculate the relative error. The result will definitely worse than the simulation due to the noise from the light source, spectrometer, data fitting and so on. Nevertheless, we are the first group optically realized the single-pixel hyperspectral camera.

8. Future Work and Conclusion

In the future, we want to integrate the RGB camera into our setup and use its measurement to further improve the reconstruction quality. For the original prototype, we want to solve the low light issue by finding more powerful and full-band light source. To reduce the frame capture time, we can optimize the DMD switching by preloading the patterns onto the board. By solving previous issues, we may try to reconstruct image with higher resolution.

References

[1] Duarte M F, Davenport M A, Takhar D, et al. Single-pixel imaging via compressive sampling[J]. IEEE Signal Processing Magazine, 2008, 25(2): 83.

[2] Gehm M E, John R, Brady D J, et al. Single-shot compressive spectral imaging with a dual-disperser architecture[J]. Optics Express, 2007, 15(21): 14013-14027.

[3] Wagadarikar A, John R, Willett R, et al. Single disperser design for coded aperture snapshot spectral imaging[J]. Applied optics, 2008, 47(10): B44-B51.

[4] Wu Y, Mirza I O, Arce G R, et al. Development of a digital-micromirror-device-based multishot snapshot spectral imaging system[J]. Optics letters, 2011, 36(14): 2692-2694.

[5] Lin X, Liu Y, Wu J, et al. Spatial-spectral encoded compressive hyperspectral imaging[J]. ACM Transactions on Graphics (TOG), 2014, 33(6): 233.

[6] Sun T, Kelly K. Compressive sensing hyperspectral imager[C]//Computational Optical Sensing and Imaging. Optical Society of America, 2009: CTuA5.

[7] Barzilai J, Borwein J M. Two-point step size gradient methods[J]. IMA Journal of Numerical Analysis, 1988, 8(1): 141-148.